SCIENTIFIC REPORTS

OPEN

SUBJECT AREAS:
POROUS MATERIALS
CATALYST SYNTHESIS

Received
30 August 2013

Accepted
29 October 2013

Published
14 November 2013

Correspondence and requests for materials should be addressed to J.G.Y. (jiaguoyu@yahoo.com) or M.J. (jaroniec@kent.edu)

Hierarchically Macro-Mesoporous Pt/γ-Al_2O_3 Composite Microspheres for Efficient Formaldehyde Oxidation at Room Temperature

Longhui Nie[1,3], Aiyun Meng[1], Jiaguo Yu[1] & Mietek Jaroniec[2]

[1]State Key Laboratory of Advanced Technology for Material Synthesis and Processing, Wuhan University of Technology, Wuhan 430070, China, [2]Department of Chemistry and Biochemistry, Kent State University, Kent, Ohio, 44242, USA, [3]School of Chemistry and Chemical Engineering, Hubei University of Technology, Wuhan 430068, China.

Room temperature catalytic oxidation by noble metals is considered to be the most promising strategy for the removal of HCHO, which is one of the major indoor air pollutants. Hierarchically macro-mesoporous structured Pt/γ-Al_2O_3 hollow spheres with open and accessible pores were synthesized and used for catalytic oxidative decomposition of HCHO at room temperature. The prepared composite hollow spheres showed higher catalytic activity than the conventional nanoparticle supports, which is mainly due to their hierarchical macro-mesoporous structure facilitating diffusion of reactants and products, and the high dispersion of accessible catalytic Pt nanoparticles. This work may contribute to the development of hierarchically structured materials and high-performance catalysts for indoor air purification and related catalytic processes.

Formaldehyde (HCHO) is one of the major indoor air pollutants and a long-term exposure to HCHO may cause health problems such as nasal tumors and skin irritation[1,2]. Room temperature catalytic oxidative decomposition of HCHO to CO_2 and H_2O is considered to be the most promising strategy for the removal of HCHO because this process is environmentally friendly and energy saving[3–5]. It overcomes disadvantages associated with relatively short lifetime of adsorbents[6,7] and additional instrumentation and operating costs of high-temperature thermal catalytic oxidation[8] and photocatalytic oxidation[9]. In the case of catalytic oxidation, a variety of supported noble metals like Pt, Pd, and Au[3,4,10,11] were used as catalysts for HCHO oxidation. Among them, the Pt-supported catalysts exhibited higher catalytic performance for decomposition of HCHO even at room temperatures. For instance, HCHO can be completely oxidized into CO_2 and H_2O on Pt/TiO_2 catalysts at room temperature[3,4,12–15]. However, the catalytic activity of Pt-supported catalysts must be further enhanced from the view point of practical use and commerce.

The morphology and structure of supports affect significantly the catalytic performance of supported catalysts. Recently, the fabrication of hierarchically macro-mesoporous materials[16–19] and hollow spheres[20–24] has received considerable attention because of both fundamental studies and practical applications. The materials with hierarchically macro-mesoporous structures are of great interest as potential catalyst supports, catalysts and sorbents, which is due to their large specific surface area and, more important, their texture mesopores and intrinsic interconnected macropore network being able to efficiently transport guest species to framework catalytic sites[18]. In addition, inorganic materials with hollow spherical structure show several advantages such as high mobility, good surface permeability, large specific area and low density[20]. So, inorganic hollow spheres with hierarchically macro-mesoporous structures are good candidates for catalyst supports. However, to date, the supported Pt catalysts for HCHO oxidation were usually synthesized using nanopartcles (NPs) as supports (such as: TiO_2, CeO_2-MnO_2, Fe_2O_3, et al.)[3,4,12,13].

γ-Al_2O_3 is an important industrial material that is widely used for preparation of catalyst supports, catalysts, adsorbents, ceramics, abrasives and filters[25–27], many of which depend on morphological characteristics such as particle/pore size, shape, and structure. Moreover, Pt/γ-Al_2O_3 catalysts were usually synthesized using γ-Al_2O_3 as support, and widely used for CO oxidation[28], ring-opening reaction of cyclopentane[29], hydrogen generation[30], and selective hydrogenation of styrene[31], diesel oxidation[32], and so on. However, hierarchically macro-mesoporous Pt/

Table 1 | Experimental conditions for the as-synthesized catalysts and their physical properties

Sample	Sample composition	Pt dispersion (%)	S_{BET} (m^2/g)	V_{pore} (cm^3/g)	d_{pore} (nm)	Pt wt%
HAO	Al_2O_3	—	149	0.45	12.3	
PHAO	Pt/Al_2O_3	74.4	114	0.37	12.8	0.41
PTO	Pt/TiO_2	48.8	41	0.24	24.0	0.40
AO	Al_2O_3	—	144	0.21	5.8	
PAO	Pt/Al_2O_3	29.2	100	0.16	6.3	0.35
HAO-BM	Al_2O_3	—	125	0.36	11.6	
PHAO-BM	Pt/Al_2O_3	29.3	119	0.30	10.1	0.40

Al_2O_3/composite microspheres have not been reported yet and used for oxidative decomposition of HCHO. The aim of this study was to further improve the catalytic activity of Pt catalyst in oxidative decomposition of HCHO by using hierarchically macro-mesoporous structured γ-Al_2O_3 hollow spheres (HAO) synthesized by a facile chemically induced self-transformation method, and then to prepare HAO materials as supports for Pt catalyst. It is shown that the resulting Pt/HAO composite catalyst (PHAO) exhibited a surprising remarkable catalytic performance towards HCHO oxidative decomposition at room temperature.

HAO support was prepared by the chemically induced self-transformation method in water using potassium aluminum sulfate and urea as the precursors at 170°C for 3 h[21]. Then, the PHAO sample was synthesized via impregnation of the as-prepared HAO with Pt precursor and $NaBH_4$-reducing agent. For the purpose of comparison, commercial TiO_2 (P25, Degussa, Germany), commercial γ-Al_2O_3 (AO) and γ-Al_2O_3 nanosheets (HAO was milled by a planetary ball mill, HAO-BM) were used as supports of Pt catalyst to obtain the Pt/TiO_2 (PTO), Pt/commercial γ-Al_2O_3 (PAO) and Pt/γ-Al_2O_3 nanosheet (PHAO-BM) catalysts with the same Pt deposition process as in the case of PHAO. The nominal weight ratio of Pt to support was fixed to 0.5 wt% and the basic parameters are shown in Table 1.

Results

XRD analysis. The XRD patterns of the HAO and PHAO samples are presented in Supplementary Fig. S1, indicating that the phase structure of the Al_2O_3 sample is gamma phase (JCPDS, No. 10-0425); in the case of these samples the position and height of Al_2O_3 diffraction peaks did not change before and after Pt deposition. Further observation indicates that no XRD diffraction peaks of Pt are observed in the PHAO sample due to its low loading (0.5 wt%), small particle size, and good dispersion[3,33].

SEM and TEM analysis. The morphology and microstructure of the HAO and PHAO samples were studied by scanning electron microscopy (SEM), transmission electron microscopy (TEM) and high-resolution transmission electron microscopy (HRTEM) (Fig. 1 and Supplementary Fig. S2). SEM images indicate that the prepared PHAO and HAO samples are hierarchical microspheres (Fig. 1a and Supplementary Fig. S2a), and their particle size is about 4–6 μm. TEM (Fig. 1b and Supplementary Fig. S2b) images reveal that the thickness of the shell wall is about 700–900 nm, and that the external surface of the spheres consisted of randomly aggregated and interconnected 10 nm-thick nanoplatelets (inset of Fig. 1a); consequently, the resulting microspheres were highly disordered porous superstructures with highly rough outer surface. A comparison of TEM images (Fig. 1b and Supplementary Fig. S2b) of the PHAO and HAO samples shows that the deposition of Pt did not change the morphology of the PHAO sample, which remained as a hollow spherical structure. High-magnification TEM image (Fig. 1c) further indicates that PHAO is composed of a large amount of nanosheets with the width of ca. 80–100 nm and thickness of about 10 nm, and many small Pt NPs with size of ca. 2–3 nm (marked by arrows in Fig. 1c) are evenly deposited on the surface of nanosheets. HRTEM image (Fig. 1d) shows that the lattice spacing in white circle is ca. 0.224 nm, consistent with the lattice spacing of (111) planes of metallic Pt NPs, confirming that the black small particles are Pt NPs[34].

N_2 sorption analysis. The porous structure and texture of the shells observed by SEM and TEM were further elucidated by N_2 sorption analysis. Nitrogen adsorption-desorption isotherms and the corresponding pore-size distribution curves for the HAO and PHAO samples are shown in Supplementary Fig. S3 and its inset, respectively. Nitrogen adsorption-desorption isotherms for above two samples are of type IV according to International Union of Pure and Applied Chemistry (IUPAC) classification[35], indicating the existence of mesopores. The adsorption branches of two isotherms resemble type II, suggesting the presence of macropores. The shape of hysteresis loops resembles type H3 at high relative pressure (P/P_0) range of 0.5–1.0, indicating the presence of slit-like pores. The isotherms show high adsorption values at relative pressures approaching 1.0, which is typical for materials with large mesopores and macropores[36]. As compared to HAO, there is a little decrease in the amount of adsorbed N_2 on PHAO at high relative pressures, 0.9–1.0, implying the smaller pore volume for the later. The pore-size distribution curves (inset in Supplementary Fig. S3) calculated from the adsorption branches of the nitrogen isotherms by the BJH method are quite broad and multimodal with smaller mesopores (peak pore

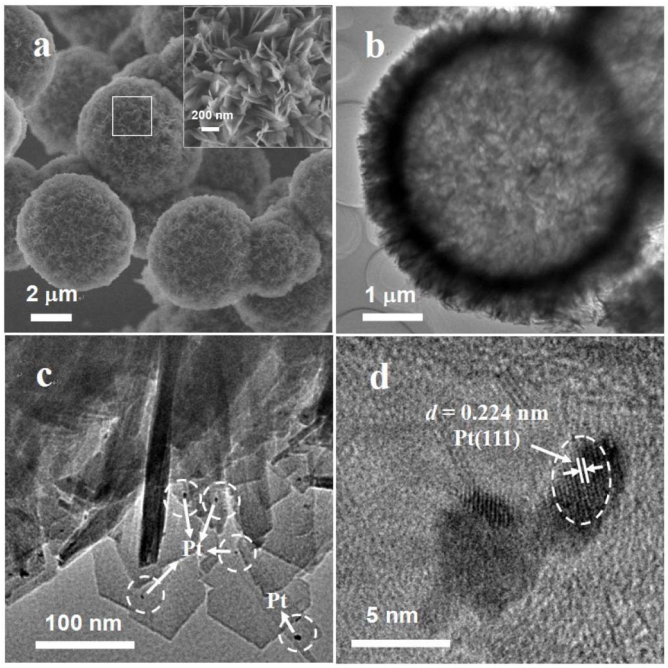

Figure 1 | Structural characterization of Pt/-γAl_2O_3. SEM (a), high-magnification SEM (inset in a), TEM (b, c) and HRTEM (d) images of the PHAO sample.

at ca. 2.0 nm) and larger pores with diameters of about 50 nm for HAO and 60 nm for PHAO, respectively. The smaller mesopores reflect pores present within nanosheets, while larger mesopores are formed between stacked nanosheets. N_2 adsorption-desorption isotherms do not provide information about macropores with sizes larger than 100 nm. Therefore, the macroporous structure of the HAO and PHAO samples was observed directly by SEM and TEM. The as-prepared HAO sample exhibited a great amount of open slit-like pores with outer pore diameters of 200–600 nm in the shell wall of hollow spheres and a cavity with diameter of 3–5 μm (Supplementary Fig. S2). After deposition of Pt NPs the macroporous structures were well preserved, and the pore size and shape did not show a visible change (Fig. 1a, b). These open macroporous channels may serve as ideal gas-transport routes for gas molecules into the interior space of alumina. Furthermore, a small decrease in the pore volume of PHAO is observed as compared to HAO. The BET surface area (S_{BET}), pore volume (V_{pore}) and pore size (d_{pore}) of the HAO and PHAO samples are listed in Table 1, indicating a slight decrease of the specific surface area and pore volume of the PHAO sample after Pt deposition as compared to the HAO sample; however, no visible difference is observed in the pore size distributions. The observed reduction in the specific surface area and pore volume of the PHAO catalyst was probably caused by two reasons: (i) The density of the Pt/Al_2O_3 samples increases due to the larger density of Pt (21.45 g/cm^3) than Al_2O_3 (3.65 g/cm^3, gamma); note that the specific surface area is expressed per gram of the sample; (ii) Pt NPs and Na^+ from $NaBH_4$ and NaOH can cover the surface of Al_2O_3 and partially block pores that leads to the observed decrease in the surface area and pore volume[3]. The large mesopores and macropores of the PHAO sample are expected to benefit the diffusion of the reactants and products during the oxidation of HCHO[3,37].

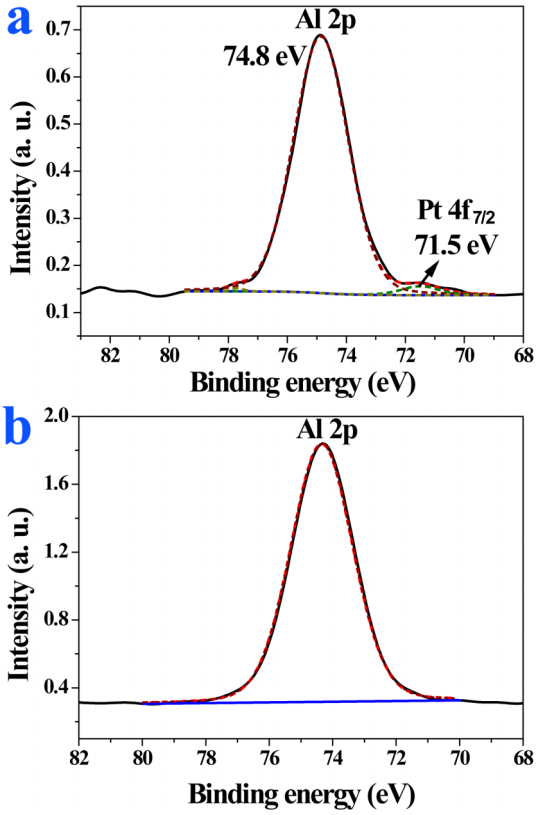

Figure 2 | Chemical states of Al and Pt atoms. High-resolution XPS spectra for Pt4*f* and Al2*p* of the PHAO (a) and HAO (b) samples.

XPS analysis. The chemical state of atoms in the prepared samples was investigated by X-ray photoelectron spectroscopy (XPS). The high-resolution XPS spectra of Pt4*f*, Al2*p* and O1*s* regions for the PHAO and HAO samples are shown in Fig. 2 and Supplementary Fig. S4. As shown in Fig. 2a, two peaks located at 71.5 and 74.8 eV are observed for the PHAO sample, which can be assigned to Pt4$f_{7/2}$ of metallic Pt[3,38,39] and Al2*p* of γ-Al_2O_3[39–41], respectively. However, the Pt4$f_{5/2}$ peak of metallic Pt is not observed, which is due to the weak peak of Pt4$f_{5/2}$ (at 74.3 eV) overlapped by the strong peak of Al2*p* (at 74.8 eV) of γ-Al_2O_3. However, only one peak for Al2*p* of the HAO sample can be observed in Fig. 2b. The results further demonstrate Pt NPs were deposited on the surface of γ-Al_2O_3.

High-resolution XPS spectrum of O 1*s* is shown in Supplementary Fig. S4. Two fitted peaks located at 531.7 and 532.8 eV are observed for the PHAO and HAO samples, which can be assigned to the lattice oxygen (O 1*s*) of Al_2O_3 and the oxygen of the surface hydroxyl (OH) groups, respectively[42,43]. It is notable that the existence of surface hydroxyls near to Pt NPs is beneficial for the oxidation of HCHO[3].

FTIR spectrum analysis. To further confirm the existence of surface hydroxyl groups, the FTIR spectra of the PHAO and HAO samples were investigated. As shown in Supplementary Fig. S5, the FTIR spectrum of the PHAO sample is similar to that of the HAO sample. The broad and intense vibration bands at 3449 cm^{-1} is associated with the stretching vibrations of the surface-adsorbed water and hydroxyl groups, while those at 1628 cm^{-1} are associated with their bending mode, confirming the existence of surface hydroxyl groups and adsorbed water. The strong and broad bands at 450–1000 cm^{-1} are associated with the special vibration of aluminium oxide[44].

Catalytic performance. The catalytic performance of the PHAO, PAO, PTO and PHAO-BM catalysts towards HCHO oxidation is shown in Fig. 3. As can be seen from this figure, the HCHO concentration (shown in Fig. 3a) decreased with increasing reaction time, and accordingly, the CO_2 concentration (shown in Fig. 3b) increased, indicating that the oxidation of HCHO into CO_2 and H_2O occurred. Also, it is noteworthy that the rates of the HCHO concentration decrease and the CO_2 concentration increase in these catalytic systems are different, indicating their different catalytic activity towards HCHO oxidation. Among the PHAO, PAO and PTO samples, when PHAO catalyst was used for HCHO oxidation, the rates of the HCHO concentration decrease and the corresponding CO_2 concentration increase are highest, indicating PHAO is the most active catalyst towards HCHO oxidation. Especially in the first 12 min, CO_2 concentration increases much faster in the presence of the PHAO sample than in the case of PAO and PTO, implying that more CO_2 was produced and CO_2 desorbs more easily and escapes from the surface of PHAO. The observed larger increase in the CO_2 concentration (about 331 ppm in 60 min) than that corresponding to the decrease in the HCHO concentration (about 155 ppm in 60 min) for the PHAO sample is due to the oxidation of some HCHO molecules desorbed from the reactor surface to CO_2 during experiment.

The stability of catalysts is also very important in their applications. The stability of PHAO in oxidative decomposition of HCHO at the room temperature was evaluated by conducting the experiment eight times on the recycled PHAO and the results are shown in Figure S6. The oxidation rate of HCHO shown in Figure S6a and the generation rate of CO_2 shown in Figure S6b over PHAO for eight repeated cycles do not show an obvious decline as compared to those obtained in the first-cycle, indicating that the PHAO catalyst can maintain a stable and efficient catalytic performance.

Discussion

Why the PHAO sample exhibits higher catalytic activity than PAO and PTO? The results of SEM, TEM, HRTEM and adsorption

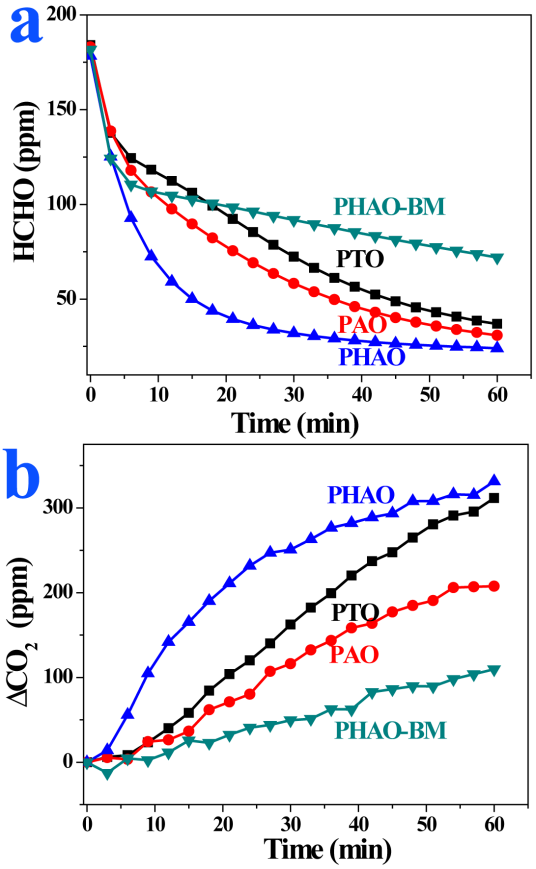

Figure 3 | Catalytic performance. Concentration changes of formaldehyde (a) and ΔCO_2 (the difference between CO_2 concentration at *t* reaction time and initial time, ppm) (b) as a function of reaction time for the PHAO, PAO, PTO and PHAO-BM samples.

analysis show that the PHAO sample is in the form of hierarchically macro-mesoporous structured hollow spheres composed of a large amount of nanosheets. Such hierarchically structured PHAO sample has higher surface area and larger pore volume than the PAO and PTO samples (see Table 1). The H_2 chemisorption data indicate the Pt dispersion on the PHAO surface is 74.4% (see Table 1), which is much higher than that (29.2 and 40.3%) of the PAO and PTO samples, implying that such hierarchical structure is favorable for the deposition of highly disperse Pt NPs. The highly dispersed Pt NPs (ca. 2–3 nm) are also directly observed by TEM (Fig. 1c). On the other hand, such a special hierarchical macro-mesoporous structured hollow spheres composed of a large amount of nanosheets not only provide a high surface area for Pt NPs but also facilitate the transport of reactants and products by minimizing the diffusion resistance[18,45]. In a typical gas-solid catalysis reaction, seven steps are necessary: (1) external diffusion of reactants, (2) internal diffusion of reactants, (3) adsorption of reactants on the surface of catalyst, (4) surface reaction and the formation of products, (5) desorption of products from the surface of catalyst, (6) internal diffusion of products and (7) external diffusion of products. In the oxidation of HCHO, besides the thermodynamic factors, dynamic conditions are important for activity of catalysts. The hierarchically macro-mesoporous structure of the PHAO sample facilitates fast diffusion and transport of reactants and products (see Fig. 4a, b) and therefore, better dynamic conditions exist for HCHO oxidation reaction. So, the PHAO sample exhibits higher catalytic activity than the PAO and PTO samples mainly due to hierarchically macro-mesoporous structure facilitating fast diffusion and transport of reactants and products, and due to high Pt dispersion resulting in higher

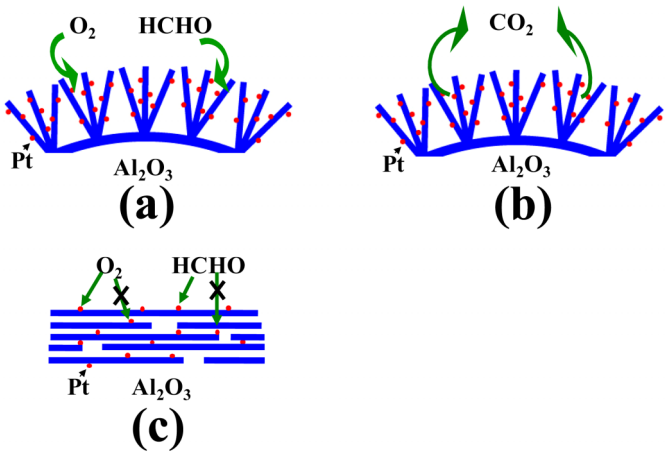

Figure 4 | Diffusion diagram. Illustration for O_2 and HCHO (a) and CO_2 (b) fast diffusion in the pore channel of PHAO catalyst, and O_2 and HCHO difficult diffusion in the pore channel of PHAO-BM catalyst (c).

concentration of catalytic active sites. Why was higher dispersion of Pt NPs achieved on HAO than on AO support? One possible explanation is that Pt NPs can be uniformly deposited on the interior and outer surface of HAO due to its hierarchical macro-mesoporous structure. In contrast, in the case of AO, Pt NPs are mainly deposited on its outer surface due to the lack of hierarchical macro-mesoporous structure.

In order to further confirm the above discussion, the HAO support was milled in a planetary ball mill to obtain the HAO-BM support and then Pt NPs were deposited onto the HAO-BM support to obtain the PHAO-BM sample. The morphology of the PHAO-BM sample is shown in Supplementary Fig. S7. The TEM image of this sample shows only a lot of overlapped nanosheets, while hollow spheres of γ-Al_2O_3 are not observed, indicating that the hierarchically hollow spheres were destroyed during the ball-milling process; also, some ca. 5–10 nm and one 30 nm aggregated Pt NP are observed in Supplementary Fig. S7a image, implying the size of Pt NPs on the PHAO-BM sample becomes larger and Pt dispersion becomes broaden after ball milling in comparison to the PHAO sample. This is easy to understand because the nucleation surface area of the PHAO-BM sample for Pt NPs decreases, which results in the growth and aggregation of Pt NPs. The Pt dispersion calculated from H_2 chemisorption data further confirms the above analysis. The Pt dispersion of PHAO-BM was only 29.3%, which is significantly smaller than that of PHAO (74.4%). The catalytic performance of the PHAO-BM sample towards HCHO oxidation is also shown in Fig. 3. For this sample, the rates of the HCHO concentration decrease and the corresponding CO_2 concentration increase are much lower than those for the PHAO sample, indicating that the catalytic activity of PHAO-BM is much lower than that of PHAO although both samples have similar surface area and pore volume (see Table 1). In the case of PHAO-BM, diffusion of O_2 and HCHO molecules is difficult in the pores formed by the stacked nanosheets (see Fig. 4c), and by poor Pt dispersion. These arguments further demonstrate that the hierarchically hollow spherical structure of the PHAO sample is important for enhancing catalytic activity towards HCHO oxidation.

In summary, hierarchically macro-mesoporous structured hollow spheres of Pt/γ-Al_2O_3 with open and accessible pores were synthesized and used for catalytic oxidative decomposition of HCHO at room temperature. The prepared catalyst possesses a high specific area, and an open and accessible pathway, and highly-dispersed Pt NPs. These features make this composite material become highly effective catalyst since the intradiffusion resistance is minimized and Pt NPs are easily accessible for reactive molecules. The hierarchically

macro-mesoporous structured Pt/γ-Al_2O_3 composite catalyst showed higher catalytic activity than the available conventional nanoparticle supports, which is mainly due to its hierarchically macro-mesoporous structure facilitating diffusion of reactants and products, and the high dispersion of accessible catalytic Pt NPs. Considering the importance and diversity of noble-metal catalysts, this work contributes to the development of hierarchically structured materials and high-performance catalysts for indoor air purification and related catalytic processes.

Methods

Preparation of hierarchically macro-mesoporous structured γ-Al_2O_3. In a typical synthesis, $KAl(SO_4)_2{\cdot}12H_2O$ (1.66 g) and $CO(NH_2)_2$ (0.42 g) powders were dissolved in 60 ml of distilled water and stirred for 10 min. The solution was placed in a 100 ml autoclave with a Teflon liner. The autoclave was maintained at 170°C for 3 h and then air cooled to room temperature. After reaction, the pH value of the solution was ca. 9.5. The white precipitate was collected and washed with distilled water and anhydrous alcohol several times. The washed precipitate was dried in a vacuum at 80°C for 12 h to acquire hierarchically macro-mesoporous structured γ-AlOOH. Then, hierarchically macro-mesoporous structured γ-Al_2O_3 was obtained by calcining γ-AlOOH at 600°C for 2 h.

Preparation of hierarchical flower-like Pt/γ-Al_2O_3 catalysts. In a typical preparation, 1 g of γ-Al_2O_3 was added into an H_2PtCl_6 solution (10 mL, 2.56 mmol/L) under magnetic stirring. After impregnation for 1 h, 2.5 mL of $NaBH_4$ (0.1 mol/L) and NaOH (0.5 mol/L) mixed solution was quickly added into the suspension under vigorous stirring for 30 min. After reduction, the suspension was evaporated at 100°C under stirring. Finally, the samples were dried at 80 °C for 6 h. The nominal weight ratio of Pt to γ-Al_2O_3 was fixed to be 0.5 wt%. For the purpose of comparison, 0.5% Pt/γ-Al_2O_3 nanosheets (HAO was milled by a planetary ball mill in 10 mL ethanol for 1 h, HAO-BM) (denoted as PHAO-BM), 0.5% Pt/TiO_2 (P25, Degussa) catalyst (denoted as PTO) and 0.5% Pt/γ-Al_2O_3 (commercial Al_2O_3, Sinopharm Chemical Reagent Co., Ltd) catalyst (denoted as PAO) were also impregnated with Pt species and subjected to $NaBH_4$-reduction. The real content of Pt in the catalysts measured by inductively coupled plasma atomic emission spectrometry (ICP-AES) was about 0.4 wt% (see Table 1).

Characterization. γ-Al_2O_3 and Pt/γ-Al_2O_3 samples were analyzed by a D/Max-RB X-ray diffractometer (Rigaku, Japan) with Cu K_α radiation at a scan rate (2θ) of 0.05° s^{-1}. Scanning electron microscopy (SEM) imaging was performed on an S-4800 field emission SEM (FESEM, Hitachi, Japan) at an accelerating voltage of 10 kV. Transmission electron microscopy (TEM) and high-resolution transmission electron microscopy (HRTEM) images were collected on a JEM-2100F microscope at an accelerating voltage of 200 kV. X-ray photoelectron spectroscopy (XPS) measurements were performed on VG ESCALAB210 with Mg $K\alpha$ source. All binding energies (BE) were referenced to the C 1s peak at 285.0 eV of the surface adventitious carbon. The Brunauer-Emmett-Teller (BET) surface area (S_{BET}) of powders was evaluated from nitrogen adsorption data recorded by using a Micromeritics ASAP 2020 nitrogen adsorption apparatus (USA). All the samples were degassed at 180°C prior to nitrogen adsorption measurements. The BET surface area was determined by a multipoint method using adsorption data in the relative pressure (P/P_0) range of 0.05–0.3. The pore size distributions were determined using adsorption data by the Barrett-Joyner-Halenda (BJH) method. The single-point pore volume was obtained from nitrogen adsorption volume at the relative pressure of 0.97. The relation between the surface area, pore volume and pore width for cylindrical pore model was used to estimate the average value of the latter. The Fourier transform infrared spectroscopy (FTIR) spectrum of Al_2O_3 was recorded on a Shimadzu IRAffinity-1 spectrometer using KBr pellets in the range of 4000–400 cm^{-1} region. Platinum dispersion was measured by H_2 chemisorption on a Micrometrics AutoChem 2920 Pulse Chemisorption System, using a thermal conductivity detector (TCD) to monitor H_2 consumption and assuming a H_2:Pt = 1 : 2 stoichiometric ratio. Prior to chemisorption, the catalyst was pretreated in flowing argon for 1 h at 200°C and then it was cooled down to ambient temperature. The chemisorption data were collected stepwise at 45°C. The platinum dispersion (D) was calculated from the H_2 chemisorption data using the following equation:

$$D = \left(\frac{V_s \times F_s \times M}{W_s \times V_m}\right) \times 100$$

where V_s is the volume of adsorbed gas (STP, standard temperature and pressure) (cm^3), F_s is the stoichiometric factor, which is equal 2 for Pt, W_s is the weight (g) of noble metal Pt, M is the molecular weight of Pt (g/mol) and V_m is the ideal gas molar volume = 22414 (cm^3/mol).

Catalytic activity test. The room-temperature catalytic oxidation of HCHO was performed in a dark organic glass box covered by a layer of aluminum foil on its inner wall at 20°C. The experimental setup is shown in our previous work[3]. 0.3 g of catalyst was dispersed on the bottom of glass petri dish with a diameter of 14 cm. After placing the sample dishes in the bottom of the reactor with a glass slide cover, 6 μL of condensed HCHO solution (38%) was injected into the reactor and a 5 watt fan was placed on the bottom of the reactor in the whole reaction process. After 2 h, the HCHO solution was volatilized completely and the concentration of HCHO was stabilized. The analysis of HCHO and CO_2 was on-line conducted by a Photoacoustic IR Multigas Monitor (INNOVA air Tech Instruments Model 1412). The HCHO vapor was allowed to reach adsorption equilibrium within the reactor prior to catalytic activity experiment. The initial concentration of HCHO after adsorption equilibrium was controlled at about 183 ppm, which remained constant until the glass slide cover on the petri dish was removed to start the catalytic oxidation reaction of HCHO. Each set of experiments was followed for about 60 min. The CO_2 concentration increase (ΔCO_2, which is the difference between CO_2 concentration at t reaction time and initial time, ppm) and HCHO concentration decrease were used to evaluate the catalytic performance.

1. Collins, J. J. *et al.* A review of adverse pregnancy outcomes and formaldehyde exposure in human and animal studies. *Regul. Toxicol. Pharm.* **34**, 17–34 (2001).
2. Salthammer, T., Mentese, S. & Marutzky, R. Formaldehyde in the indoor environment. *Chem. Rev.* **110**, 2536–2572 (2010).
3. Nie, L. H. *et al.* Enhanced performance of NaOH-Modified Pt/TiO_2 toward room temperature selective oxidation of formaldehyde. *Environ. Sci. Technol.* **47**, 2777–2783 (2013).
4. Zhang, C. B. *et al.* Alkali-metal-promoted Pt/TiO_2 opens a more efficient pathway to formaldehyde oxidation at ambient temperatures. *Angew. Chem. Int. Ed.* **51**, 9628–9632 (2012).
5. Huang, H. B. & Leung, D. Y. C. Complete elimination of indoor formaldehyde over supported Pt catalysts with extremely low Pt content at ambient temperature. *J. Catal.* **280**, 60–67 (2011).
6. Xu, Z. H. *et al.* Microemulsion-assisted synthesis of hierarchical porous Ni$(OH)_2$/SiO_2 composites toward efficient removal of formaldehyde in air. *Dalton Trans.* **42**, 10190–10197 (2013).
7. Xu, Z. H., Yu, J. G. & Xiao, W. Microemulsion-assisted preparation of a mesoporous ferrihydrite/SiO_2 composite for the efficient removal of formaldehyde from air. *Chem. Eur. J.* **19**, 9592–9598 (2013).
8. Scirè, S. *et al.* Catalytic combustion of volatile organic compounds on gold/cerium oxide catalysts. *Appl. Catal. B* **40**, 43–49 (2003).
9. Yu, J. G. *et al.* Preparation, characterization and photocatalytic activity of in situ N,S-codoped TiO_2 powders. *J. Mol. Catal. A: Chem.* **246**, 176–184 (2006).
10. Huang, H. B. & Leung, D. Y. C. Complete oxidation of formaldehyde at room temperature using TiO_2 supported metallic Pd nanoparticles. *ACS Catal.* **1**, 348–354 (2011).
11. Ma, C. Y. *et al.* Investigation of formaldehyde oxidation over Co_3O_4–CeO_2 and Au/Co_3O_4–CeO_2 catalysts at room temperature: effective removal and determination of reaction mechanism. *Environ. Sci. Technol.* **45**, 3628–3634 (2011).
12. Tang, X. F. *et al.* Pt/MnO_x-CeO_2 catalysts for the complete oxidation of formaldehyde at ambient temperature. *Appl. Catal. B* **81**, 115–121 (2008).
13. An, N. H. *et al.* Complete oxidation of formaldehyde at ambient temperature over supported Pt/Fe_2O_3 catalysts prepared by colloid-deposition method. *J. Hazard. Mater.* **186**, 1392–1397 (2011).
14. Zhang, C. B., He, H. & Tanaka, K. Perfect catalytic oxidation of formaldehyde over a Pt/TiO_2 catalyst at room temperature. *Catal. Commun.* **6**, 211–214 (2005).
15. Zhang, C. B., He, H. & Tanaka, K. Catalytic performance and mechanism of a Pt/TiO_2 catalyst for the oxidation of formaldehyde at room temperature. *Appl. Catal. B* **65**, 37–43 (2006).
16. Imhof, A. & Pine, D. J. Ordered macroporous materials by emulsion templating. *Nature* **389**, 948–951 (1997).
17. Fang, W. Q. *et al.* Hierarchical structures of single-crystalline anatase TiO_2 nanosheets dominated by {001} facets. *Chemi. Eur. J.* **17**, 1423–1427 (2011).
18. Yu, J. G., Su, Y. R. & Cheng, B. Template-free fabrication and enhanced photocatalytic activity of hierarchical macro-/mesoporous titania. *Adv. Funct. Mater.* **17**, 1984–1990 (2007).
19. Yu, J. G. *et al.* Hydrothermal preparation and photocatalytic activity of hierarchically sponge-like macro-/mesoporous titania. *J. Phys. Chem. C* **111**, 10582–10589 (2007).
20. Yu, J. G. *et al.* Fabrication of hollow inorganic microspheres by chemically induced self-transformation. *Adv. Funct. Mater.* **16**, 2035–2041 (2006).
21. Cai, W. Q., Yu, J. G. & Mann, S. Template-free hydrothermal fabrication of hierarchically organized γ-AlOOH hollow microspheres. *Microporous and Mesoporous Mater.* **122**, 42–47 (2009).
22. Liu, S. W., Yu, J. G. & Jaroniec, M. Tunable photocatalytic selectivity of hollow TiO_2 microspheres composed of Anatase Polyhedra with Exposed {001} Facets. *J. Am. Chem. Soc.* **132**, 11914–11916 (2010).
23. Zhu, J. X. *et al.* Hierarchical hollow spheres composed of ultrathin Fe_2O_3 nanosheets for lithium storage and photocatalytic water oxidation. *Energy Environ. Sci.* **6**, 987–993 (2013).
24. Han, L. J. *et al.* Controlled synthesis of double-shelled CeO_2 hollow spheres and enzyme-free electrochemical bio-sensing properties for uric acid. *J. Mater. Chem.* **22**, 17079–170825 (2012).
25. Shafi, K. V. P. M. *et al.* A new route to alumoxane gel: a versatile precursor to γ-alumina and alumina-based ceramic oxides. *J. Am. Chem. Soc.* **125**, 4010–4011 (2003).

26. Zhang, Z. R. *et al*. Mesostructured forms of γ-Al_2O_3. *J. Am. Chem. Soc.* **124**, 1592–1593 (2002).
27. Paglia, G., Božin, E. S. & Billinge, S. J. L. A novel fine-scale nanostructure in gamma-Al_2O_3. *Chem. Mater.* **18**, 3242–3248 (2006).
28. Tankov, I. *et al*. DRIFTS study of CO adsorption on praseodymium modified Pt/Al_2O_3. *Appl. Surf. Sci.* **259**, 831–839 (2012).
29. Shi, H. *et al*. Catalytic consequences of particle size and chloride promotion in the ring-opening of cyclopentane on Pt/Al_2O_3. *ACS Catal.* **3**, 328–338 (2013).
30. He, L. *et al*. Surface modification of Ni/Al_2O_3 with Pt: Highly efficient catalysts for H_2 generation via selective decomposition of hydrous hydrazine. *J. Catal.* **298**, 1–9 (2013).
31. Betti, C. *et al*. Effect of the sequence of impregnation on the activity and sulfur resistance of Pt–Ni/γ-Al_2O_3 bimetallic catalysts for the selective hydrogenation of styrene. *Appl. Catal. A* **435–436**, 181–186 (2012).
32. Kolli, T. J. *et al*. The activity of Pt/Al_2O_3 diesel oxidation catalyst after sulphur and calcium treatments. *Catal. Today* **154**, 303–307 (2010).
33. Peng, J. X. & Wang, S. D. Performance and characterization of supported metal catalysts for complete oxidation of formaldehyde at low temperatures. *Appl. Catal. B* **73**, 282–291 (2007).
34. Shang, N. *et al*. Platinum integrated graphene for methanol fuel cells. *J. Phys. Chem. C* **114**, 15837–15841 (2010).
35. Sing, K. S. W. *et al*. Reporting physisorption data for gas/solid systems with special reference to the determination of surface area and porosity. *Pure Appl. Chem.* **54**, 2201–2218 (1982).
36. Yu, J. G., Liu, W. & Yu, H. G. A One-pot approach to hierarchically nanoporous titania hollow microspheres with high photocatalytic activity. *Cryst. Growth Des.* **8**, 930–934 (2008).
37. Su, L. L. *et al*. Creating mesopores in ZSM-5 zeolite by alkali treatment: a new way to enhance the catalytic performance of methane dehydroaromatization on Mo/HZSM-5 catalysts. *Cataly. Lett.* **91**, 155–167 (2003).
38. Yu, J. G., Qi, L. F. & Jaroniec, M. Hydrogen production by photocatalytic water splitting over Pt/TiO_2 nanosheets with exposed (001) facets. *J. Phys. Chem. C* **114**, 13118–13125 (2010).
39. Moulder, J. F., Stickle, W. F., Sobol, P. E., Bomben, K. D. & Chastain, J. Eds. Handbook of X-ray Photoelectron Spectroscopy; (Pekin-Elmer Inc. Physical Electronics Division: Eden Prairie, MN, 1992).
40. Tan, B. J., Klabunde, K. J. & Sherwood, P. M. A. XPS studies of solvated metal atom dispersed catalysts. evidence for layered cobalt-manganese particles on alumina and silica. *J. Am. Chem. Soc.* **113**, 855–861 (1991).
41. Marchesini, F. A. *et al*. Spectroscopic and catalytic characterization of Pd–In and Pt–In supported on Al_2O_3 and SiO_2, active catalysts for nitrate hydrogenation. *Appl. Catal. A* **348**, 60–70 (2008).
42. Dhonge, B. P. *et al*. Synthesis of Al_2O_3 thin films using laser assisted spray pyrolysis (LASP). *Appl. Surf. Sci.* **265**, 257–263 (2013).
43. Logar, M., Kocjan, A. & Dakskobler, A. Photocatalytic activity of nanostructured γ-Al_2O_3/TiO_2 composite powder formed via a polyelectrolyte-multilayer-assisted sol–gel reaction. *Mater. Res. Bull.* **47**, 12–17 (2012).
44. Costa, T. M. H. *et al*. Study of nanocrystalline γ-Al_2O_3 produced by high-pressure compaction. *J. Phys. Chem. B* **103**, 4278–4284 (1999).
45. Yu, J. G. *et al*. Effects of acidic and basic hydrolysis catalysts on the photocatalytic activity and microstructures of bimodal mesoporous titania. *J. Catal.* **217**, 69–78 (2003).

Acknowledgments

The work was partially supported by the 863 Program (2012AA062701), 973 Program (2013CB632402), NSFC (51072154, 21177100 and 51272199), National Science Fund for Post-doctoral Scientists of China (2012M511292) and Fundamental Research Funds for the Central Universities (2013-VII-030) and Self-determined and Innovative Research Funds of SKLWUT (2013-ZD-1).

Author contributions

L.H.N. and J.G.Y. conceived the experiment. L.H.N. and A.Y.M. performed the measurements. All authors contributed to designing the experiment. L.H.N., J.G.Y. and M.J. wrote the manuscript together, and all authors contributed to revisions.

Additional information

Supplementary information accompanies this paper at http://www.nature.com/scientificreports

Competing financial interests: The authors declare no competing financial interests.

How to cite this article: Nie, L.H., Meng, A.Y., Yu, J.G. & Jaroniec, M. Hierarchically Macro-Mesoporous Pt/γ-Al_2O_3 Composite Microspheres for Efficient Formaldehyde Oxidation at Room Temperature. *Sci. Rep.* **3**, 3215; DOI:10.1038/srep03215 (2013).